The Astronomical Journal, 136:389–399, 2008 July doi:10.1088/0004-6256/136/1/389

THE ARECIBO ARP 220 SPECTRAL CENSUS. I. DISCOVERY OF THE PRE-BIOTIC MOLECULE METHANIMINE AND NEW CM-WAVELENGTH TRANSITIONS OF OTHER MOLECULES

C. J. Salter, T. Ghosh, B. Catinella[1], M. Lebron[2], M. S. Lerner, R. Minchin, and E. Momjian[3]
Arecibo Observatory, HC 03 Box 53995, Arecibo 00612, Puerto Rico; csalter@naic.edu
Received 2007 December 14; accepted 2008 April 22; published 2008 June 12

ABSTRACT

An on-going Arecibo line search between 1.1 and 10 GHz of the prototypical starburst/megamaser galaxy, Arp 220, has revealed a spectrum rich in molecular transitions. These include the "pre-biotic" molecules: methanimine (CH_2NH) in emission, three $v_2 = 1$ direct l-type absorption lines of HCN, and an absorption feature likely to be from either ^{18}OH or formic acid (HCOOH). In addition, we report the detection of two, possibly three, transitions of $\lambda 4$ cm excited OH not previously detected in Arp 220 which are seen in absorption, and a possible absorption feature from the 6.668 GHz line of methanol. This marks the first distant extragalactic detection of methanimine, a pre-biotic molecule. Also, if confirmed, the possible methanol absorption line presented here would represent the first extragalactic detection of methanol at a distance further than 10 Mpc. In addition, the strong, previously undetected, cm-wave HCN $v_2 = 1$ direct l-type lines will aid the study of dense molecular gas and active star-forming regions in this starburst galaxy.

Key words: galaxies: individual (Arp 220) – galaxies: ISM – galaxies: starburst – radio lines: galaxies

1. INTRODUCTION

Star formation in galaxies occurs in two modes: "quiescent," in which stars form at a relatively modest rate over a long period of time across the entire galaxy disk, and "starburst," in which gas is turned into stars extremely rapidly, confined to compact regions of the galaxy, often its circumnuclear volume (Kennicutt 1998). Starbursts are often triggered by external dynamical disturbances such as galaxy mergers. The dust heating associated with these intense bursts of star formation within giant molecular clouds can produce hugely increased infrared (IR) luminosity and conditions favorable for maser emission. The strong 18 cm OH megamaser emission in some of these galaxies is many orders of magnitude more luminous than its counterparts in our Galaxy (Baan et al. 1982; Baan 1989; Martin et al. 1989; Lonsdale et al. 1998; Darling & Giovanelli 2002). Ultra-Luminous Infrared Galaxies (ULIRGs) are thought to be systems where all of these processes occur simultaneously (Elston et al. 1985; Lawrence et al. 1986; Sanders & Mirabel 1996). The existence of obscured active galactic nuclei (AGNs) in these objects is also considered as an alternative (or additional) energy source where these are fueled by molecular gas falling into the central regions of the merging systems (Surace & Sanders 1999; Scoville et al. 2000; Sanders & Mirabel 1996; Genzel et al. 1998; Lutz et al. 1999; Veilleux et al. 2002, 2006; Armus et al. 2007; Imanishi et al. 2007a). Molecular gas is thus one of the most important constituents of the interstellar medium (ISM) and plays a critical role in the evolution of galaxies.

To date, over 140 molecules have been identified in space, mostly in the ISM of the Milky Way. Some of these are rather complex, containing as many as 8 to 13 atoms. Interstellar organic molecules are thought to form mostly on the surface of dust grains. Heating events, such as the formation of a protostar, release the icy grain mantles into the gas phase (Nomura & Millar 2004; Caselli et al. 1993). Once released, these molecules may form amino acids by the combination of organic species known as "pre-biotic" molecules (Blagojevic et al. 2003). (We note that non-gas phase reaction pathways for the formation of extraterrestrial amino acids have been described in Elsila et al. 2007). Methanimine is one such molecule (CH_2NH; Kirchoff et al. 1973) which can form the simplest amino acid, glycine (NH_2CH_2COOH), either by (i) first combining with hydrogen cyanide (HCN) to form aminoacetonitrile (NH_2CH_2CN), with subsequent hydrolysis (Strecker Synthesis; Dickerson 1978), or (ii) directly combining with formic acid (HCOOH) (Godfrey et al. 1973). Methanimine has been previously detected in the interstellar medium of our own Galaxy (Godfrey et al. 1973; Dickens et al. 1997) and tentatively in the nearby galaxy, NGC 253 (Martín et al. 2006), but never beyond the neighborhood of our Galaxy (i.e. beyond ∼5 Mpc).

The majority of interstellar molecules (both galactic and extragalactic) have been discovered at millimetric wavelengths, as molecules with small moments of inertia are the most abundant cosmically, with their rotational lines occurring at mm or shorter wavelengths. However, although less abundant, many complex molecules have spectral lines in the radio regime for $\lambda > 3$ cm, where "line confusion" does not set a limit to their detectability. Many transitions of small polycyclic aromatic hydrocarbons (PAHs), pre-biotic molecules, and even a number of transitions of the simplest amino acid, glycine, fall within the relatively unexplored spectral range between 1 and 10 GHz. In addition, observations in this frequency range are complementary to mm spectral-line surveys which probe colder, lower-density gas.

At Arecibo, we are conducting a spectral-line census of Arp 220 between 1.1 and 10 GHz, for which the initial observations took place between 2007 March 31 and 2007 April 22. It is planned that the remaining observations will be made in 2008. Here we report the discovery of methanimine emission in this galaxy, plus the detection of three $v_2 = 1$ direct l-type absorption lines of HCN (Thorwirth et al. 2003) from the $J = 4$, 5, and 6 vibrational levels. Also reported is the possible detection of another pre-biotic molecule, formic acid,

[1] Also at: MPIfA, Karl-Schwarzschild-Straße 1, Postfach 1317, D-85741, Garching, Germany.
[2] Also at: Department of Physical Sciences, University of Puerto Rico, P.O. Box 23323, San Juan 00931-3323, Puerto Rico.
[3] Also at: NRAO, Array Operations Center, P.O. Box O, 1003 Lopezville Road, Socorro, NM 87801-0387, USA.

albeit not unambiguously due to the presence of a nearby ^{18}OH line. In addition, we present the first detections of two, possibly three, λ4 cm transitions of the OH radical in absorption, high signal-to-noise ratio (S/N) detections of the λ6 cm and 5 cm transitions of OH, and the possible detection of the 6.7 GHz methanol (CH_3OH) transition in absorption.

2. ARP 220

At a distance of ∼77 Mpc (redshift, $z = 0.018126$), Arp 220 is the nearest ULIRG. Much of its IR luminosity arises from a powerful, dust-enshrouded starburst, triggered by the merger of two gas-rich galaxies (Sakamoto et al. 1999; Mundell et al. 2001; Sanders & Mirabel 1996). Evidence for this is provided by high-resolution optical and radio images revealing a double nucleus with tidal tails and dust lanes. A high supernova rate has been found from recent high-resolution very long baseline interferometry (VLBI) studies (Lonsdale et al. 2006). Molecules such as the OH radical (Baan et al. 1982; Ghosh et al. 2003), CO (Scoville et al. 1986), formaldehyde (Araya et al. 2004), ammonia (Takano et al. 2005), and mm-transitions of HCN (Solomon et al. 1992; Evans et al. 2006; Imanishi et al. 2007b) have been detected in Arp 220. In fact, Downes & Eckart (2007) have recently used high-resolution imaging of the CO(2–1) line and the λ1.3 mm dust radiation to provide strong evidence for the existence of a "buried" AGN in the western nucleus of the galaxy, a conclusion heavily affecting interpretation of the situation within Arp 220.

Arp 220 is also known as the prototype OH megamaser galaxy. Its OH λ18 cm maser emission was first reported by Baan et al. (1982). High-resolution maps of the OH maser revealed complex structures which could be interpreted either as a dual-component distribution (Diamond et al. 1989; Lonsdale et al. 1998; Rovilos et al. 2003) or by clumpy unsaturated masers within a single-component medium (Parra et al. 2005; Momjian et al. 2006).

3. OBSERVATIONS

Using several of the complement of receivers on the Arecibo 305 m telescope, we are in the process of making an almost-complete spectral scan of Arp 220 between 1.1 and 10 GHz. To do this, we have employed the Wideband Arecibo Pulsar Processor (WAPP) spectrometer in its recently commissioned "dual-board" mode. In this mode, eight independent boards, each of 100 MHz bandwidth with three-level quantization, can be used to cover a spectral band of up to 800 MHz at a single time. Compared to the earlier WAPP capacity, this doubles the total bandwidth covered. The present project serves both for the scientific commissioning of this new option and as a demonstration of its capabilities.

In practice, we have overlapped the eight boards for each observation such that their centers are separated by 85 MHz. As the final ∼5 MHz are affected by filter roll-off, this allows high-quality data to be acquired for an instantaneous bandwidth of 680 MHz, meaning that those Arecibo receivers which have total bandwidths of 2 GHz can be fully covered via three separate frequency settings. The basic spectral resolution is 24.4 kHz, and both orthogonal polarizations of the celestial signal are recorded.

The observations are being made via a modified version of the Double Position Switching (DPS) technique (Ghosh & Salter 2002). An ON/OFF position-switched observation with 5 min component phases is made on Arp 220, followed by an ON/OFF with 1 min phases on the strong, angularly nearby, continuum source, J1531+2402, which is used as a bandpass calibrator. In the presence of bandpass ripples or trapped modes in the orthomode transducer of the feed, this strategy is necessary at all frequencies to produce acceptable spectral baselines. In addition, apparent features observed in the data can often be recognized as astronomical, and not due to the presence of radio frequency interference (RFI), via a comparison of the spectra for Arp 220 and J1531+2402. Data for a total ON-source observing time of about 60 min for Arp 220 will eventually be acquired for each frequency setting.

Data reduction has been performed using the Arecibo IDL analysis package written by Phil Perillat. The individual ON/OFF scans on Arp 220 were processed to yield (ON–OFF)/OFF spectra, and these were "bandpass corrected" using similar spectra for J1531+2402. Each individual Arp 220 and J1531+2402 scan was inspected for quality, and all RFI present was noted. A number of scans were rejected either due to technical problems or because of excessive RFI. All acceptable scans for a particular frequency setting were then co-added to produce the final spectra. These spectra were smoothed in frequency to a number of resolutions, and the resultant spectra were inspected visually to identify the presence of possible emission or absorption lines. Considerable cross-checking was performed to ensure that candidate lines were real and not the effect of RFI or equipment problems.

4. RESULTS AND DISCUSSION

A complete cm-wavelength line census for Arp 220 and its full implications for the physical and chemical properties of the interstellar medium of this galaxy are deferred until completion of the observations. Here we present the detection of methanimine in emission, and of the $v_2 = 1$ direct l-type transitions of HCN, excited-OH transitions, a line that could be either ^{18}OH or HCOOH, and possibly methanol in absorption for this prototypical nearby ULIRG. The spectra are presented in Figures 1–10, and the parameters derived from them are given in Tables 1 and 2.

Table 1 presents the results for the emission line of methanimine. The table is ordered as follows: Columns 1–3 present the name of the molecule, the relevant transition, and its rest frequency in MHz. Column 4 is the peak flux density of the line in mJy. Column 5 is the root mean square (rms) noise on the spectrum in mJy at a velocity resolution of ∼30 km s^{-1}. Column 6 is the radial velocity in km s^{-1} at the peak of the measured line, derived from the rest frequency of the strongest of the six lines in the multiplet (i.e., that at 5289.813 MHz). Column 7 is the full-velocity width in km s^{-1} of the entire emission feature at half of the peak intensity.

Table 2 presents the results for lines seen in absorption. The table is ordered as follows. Columns 1–3 are as for Table 1. Column 4 is the maximum optical depth of the absorption line. Column 5 is the rms noise on the optical-depth spectrum at a velocity resolution of ∼30 km s^{-1}. Column 6 is the radial velocity in km s^{-1} at the maximum optical depth. Column 7 is the full width in km s^{-1} of the line at half of the peak optical depth. Column 8 is $\int \tau dV$, the integrated area in km s^{-1} under the absorption feature.

In the following sections, we discuss the spectra of each molecule separately.

4.1. Methanimine (CH_2NH)

The broad emission feature covering all six 1_{10}–1_{11} transitions of the C-band multiplet of methanimine is presented in

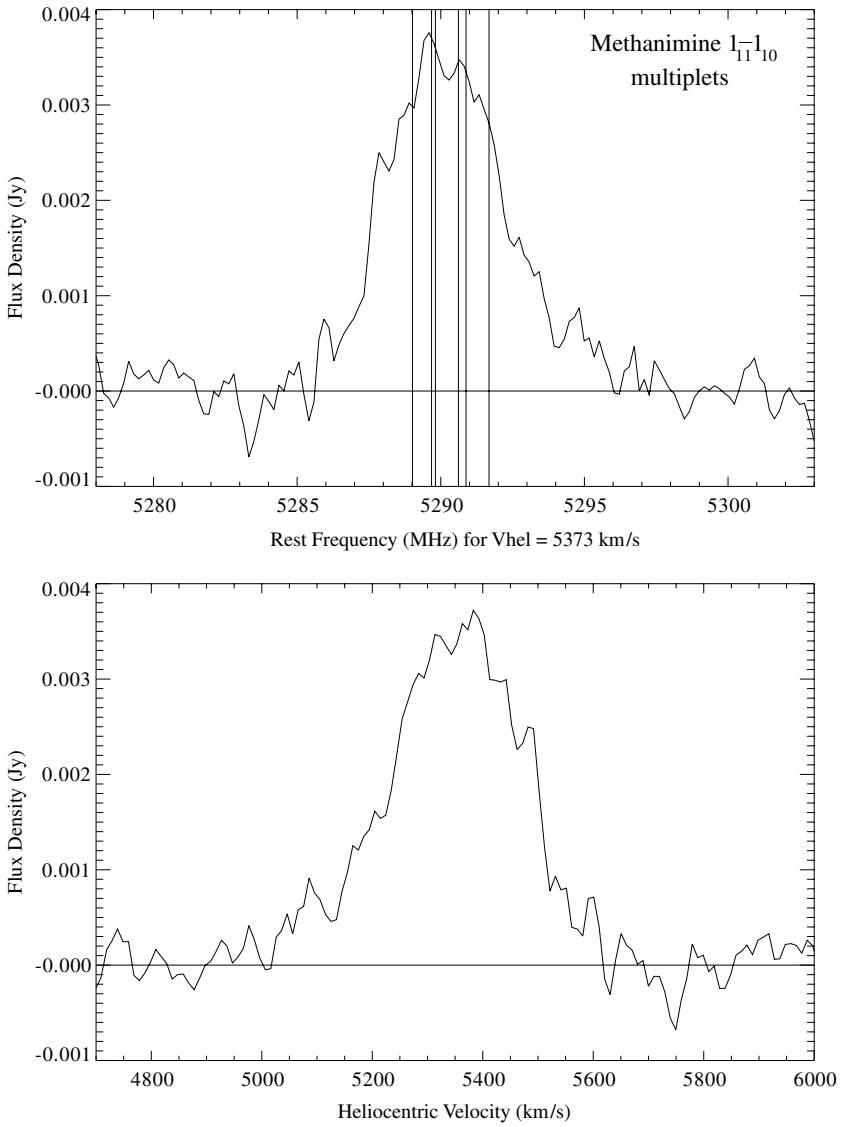

Figure 1. The blended emission line from the six 1_{10}–1_{11} multiplet transitions of methanimine in Arp 220. The rest frequencies of the individual transitions are shown by vertical lines in the upper panel for an assumed heliocentric velocity of 5373 km s^{-1} (corresponding to the western nucleus of the galaxy). The lower panel shows the same spectrum as a function of the heliocentric velocity appropriate for the strongest line (rest frequency = 5289.813 MHz) in the multiplet. The velocity resolution is ∼30 km s^{-1}.

Table 1
Derived Parameters for the Emission Multiplet of Methanimine (CH_2NH)

Molecule	Transition	Rest frequency (MHz)	S_p [a] (mJy)	σ (mJy)	v_p [a] (km s^{-1})	FWHM (km s^{-1})
Methanimine (CH_2NH)	1_{10}–1_{11}, $\Delta F = 0, \pm 1$	5289.813[b]	3.5	0.22	5362	270

Notes.
[a] The subscript p stands for "peak."
[b] The strongest of the six lines of this multiplet has this frequency in laboratory measurements.

Figure 1. In Figure 1(a), the rest frequencies of the transitions in the frame of Arp 220 were derived using a recessional velocity of 5373 km s^{-1}, as found for the western component of the OH megamaser emission of Arp 220, while the heliocentric velocity axis of Figure 1(b) is for the transition expected to be the strongest in the methanimine multiplet, that at a rest frequency of 5289.813 MHz (Godfrey et al. 1973). The total velocity width (FWHM) of this emission line is 270 km s^{-1}; we note that a large velocity width is observed for almost all molecular spectra in Arp 220 (e.g., Takano et al. 2005). Using the angular size of $0.27'' \times 0.21''$ measured for the strongest component of the formaldehyde (H_2CO) emission (Baan & Haschick 1995) as an upper limit for the angular size of the methanimine emission region, we derive a lower limit to the brightness temperature of ∼2800 K. Taking into account the six lines in the multiplet and their relative intensities, we calculate a reduced value of this lower limit to be ∼1000 K for the strongest component. This is similar to the methanimine decomposition temperature

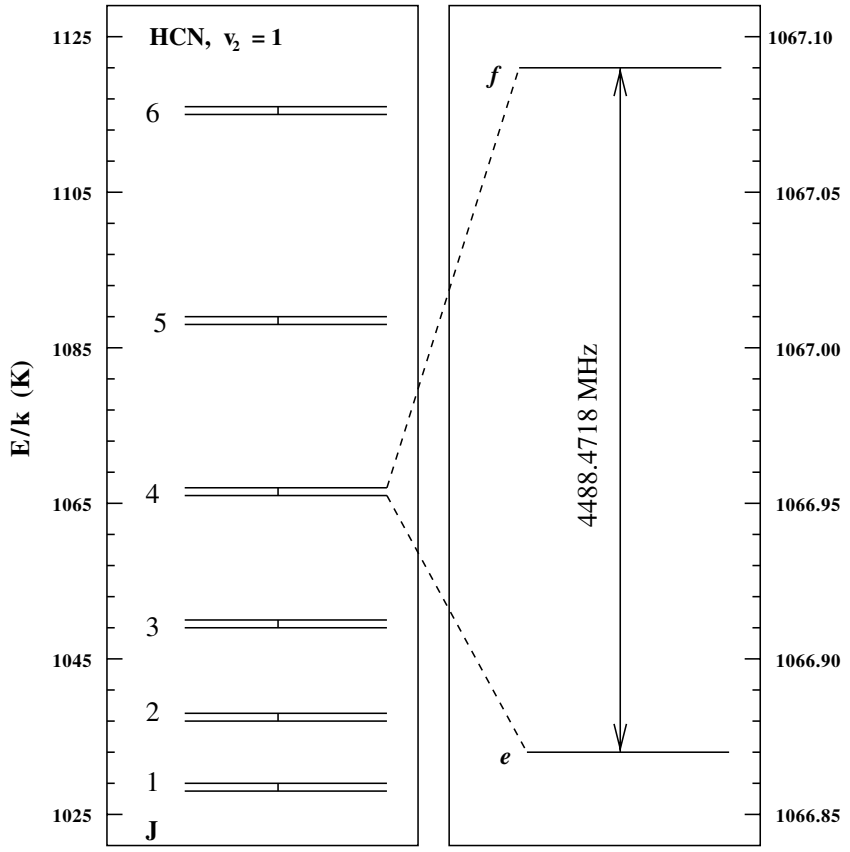

Figure 2. Term value diagram for HCN in its $v_2 = 1$ vibrational state from $J = 1$ to $J = 6$. Only the direct l-type transitions with $\Delta J = 0$ are shown. The diagram on the right-hand side shows the $J = 4$ direct l-type transition at 4488.4718 MHz in detail. We have currently observed the $J = 2, 4, 5,$ and 6 transitions at 1346, 4488, 6731, and 9423 MHz respectively (see Figure 3). This diagram was drawn using the energy level values obtained from the CDMS database (Müller et al. 2001, 2005).

Table 2
Derived Parameters from the Molecular Absorption Lines

Molecule	Transition	Rest frequency (MHz)	τ_p [a]	σ_τ	v_p [a] (km s^{-1})	FWHM (km s^{-1})	$\int \tau dV$ (km s^{-1})
Hydrogen cyanide (HCN)	$v_2 = 1,\ \Delta J = 0,\ J = 2$	1346.7650	<0.0025	0.00085	...	...	...
	$J = 4$	4488.4718	0.016	0.0009	5407	363	5.22
	$J = 5$	6731.9098	0.0205	0.001	5404	330	5.02
	$J = 6$	9423.3338	0.0268	0.002	5398	202	6.14
Hydroxyl radical (OH)	$2\Pi_{1/2},\ J = 1/2,\ F = 0$–1	4660.242	0.0254	0.00082	5425	300	7.99
	$F = 1$–1	4750.656	0.0549	0.00080	5429	287	15.91
	$F = 1$–0	4765.562	0.0295	0.00080	5447	281	8.41
	$2\Pi_{3/2},\ J = 5/2,\ F = 2$–3	6016.746[b]	0.0086	0.0016	5313	...	...
	$F = 2$–2	6030.747[c]	0.11	0.0016	5425	480	56.20
	$F = 3$–3	6035.092[c]					
	$F = 3$–2	6049.084	<0.0033	...	...	...	...
	$2\Pi_{1/2},\ J = 3/2,\ F = 1$–1	7761.747	0.0087	0.0018	5359	296	2.62
	$F = 2$–2	7820.125	0.0162	0.00153	5432	321	5.04
	$2\Pi_{1/2},\ J = 5/2,\ F = 2$–2	8135.870[b]	<0.01	0.0021	...	...	...
^{18}OH *or*	$2\Pi_{3/2},\ J = 3/2,\ F = 2$–2	1639.503	0.019	0.00137	5265	~192	...[d]
Formic acid (HCOOH)	1(1,0)–1(1,1)	*or* 1638.805			5135		
Methanol (CH_3OH)	5_1–6_0A^+	6668.5192	0.0077	0.0013	5384	360	2.53

Notes.
[a] The subscript p stands for "peak."
[b] For these low S/N detections, some of the parameters were not estimated.
[c] Since the two main lines $F = 2$–2 and 3–3 are blended, values presented here are for the two lines combined together.
[d] Since the identification of this absorption feature is ambiguous, an optical-depth integral was not estimated for it.

of 1300 K (Nguyen et al. 1996). If the solid angle of the emission is smaller than the above, for instance if the emission comes from a number of very compact components, then the brightness temperature could be much higher. We conclude that, as for formaldehyde (Araya et al. 2004), methanimine in Arp 220 is likely to be showing weak maser emission for this transition. We have been awarded time with the MERLIN array to observe this source at higher spatial resolution in order to determine the

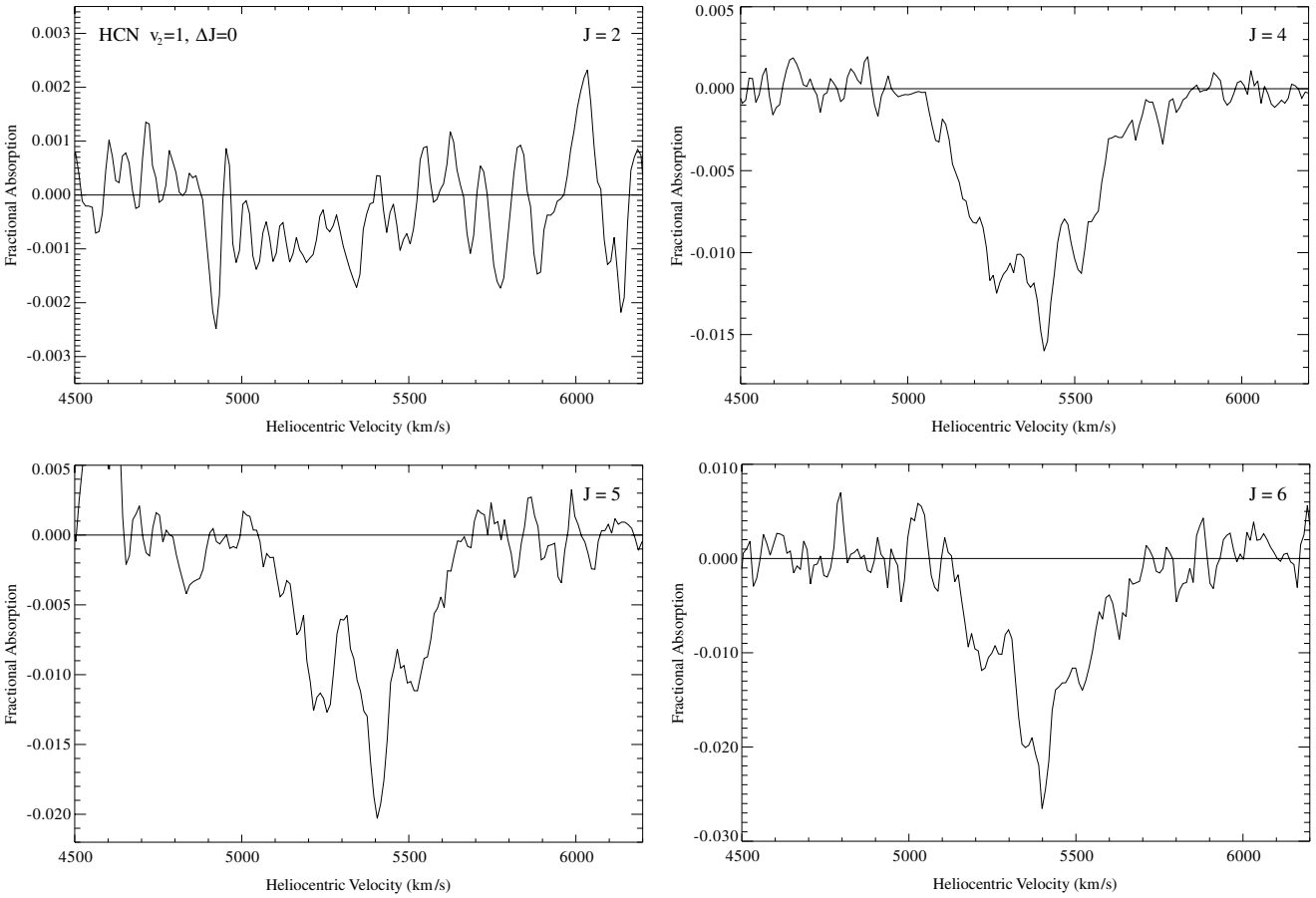

Figure 3. The first astronomical detections of the $v_2 = 1$ direct l-type absorption lines of HCN with vibrational levels $J = 4$, 5, and 6 (at 4488, 6731, and 9423 MHz respectively). The spectra are plotted with heliocentric velocity as abscissa. The non-detection of the $J = 2$ vibrational level (at 1346 MHz) is also included in the figure. The velocity resolution is ∼30 km s^{-1}.

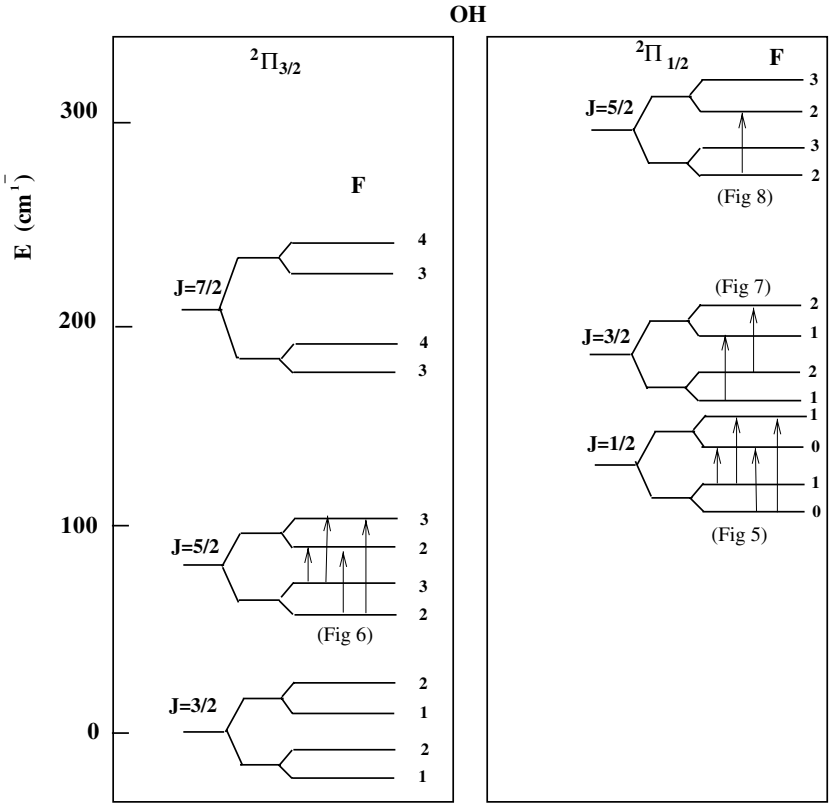

Figure 4. The energy diagram (not to scale) for various Λ-doublet transitions of the OH radical. The transitions that we have detected (all in absorption) are shown by upward-directed arrows, with the relevant figure numbers also marked. We note that $2\Pi_{1/2}$, $J = 1/2$, $F = 0$–0 and 1–1 have identical transition energies.

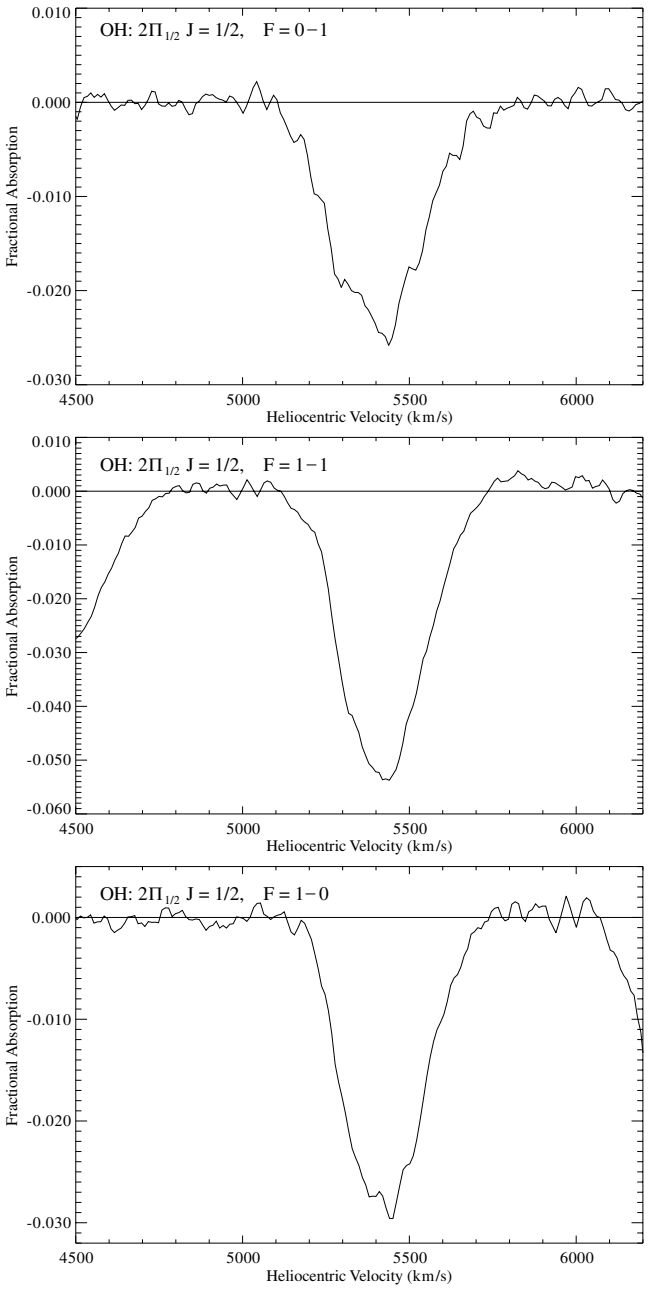

Figure 5. The three λ6 cm excited OH transitions from $2\Pi_{1/2}$, $J = 1/2$, $F =$ 0–1, 1–1/0–0, and 1–0 (at 4660, 4750, and 4765 MHz respectively). The spectra are plotted with heliocentric velocity as abscissa. The $F = 1$–1/0–0 line is about twice as strong as the other two lines. The velocity resolution is ∼30 km s^{-1}.

brightness temperature more accurately and to discover where exactly in the galaxy the emission is located.

4.2. Hydrogen Cyanide (HCN)

Figure 2 shows the energy diagram for the $v_2 = 1$ direct l-type transitions of hydrogen cyanide (HCN) in the $J = 1$ to $J = 6$ vibrational levels. Our spectra of the $J = 2$, 4, 5, and 6 HCN transitions are presented in Figure 3. The $J = 4$, 5, and 6 transitions are detected in absorption against the continuum emission of Arp 220, and we place an upper limit at the 3σ level of 0.0025 for the optical depth of the $J = 2$ line. The first detailed study of this type of HCN transition was carried out for the Galactic proto-planetary nebula, CRL 618, by Thorwirth et al. (2003). These observers detected a number of the higher vibrational levels in this HCN ladder ($J = 8$–14). However, we note that the lower-energy transitions presented here seem not to have been previously detected in any celestial source. We also note that these lines represent a high excitation energy above the HCN ground state (e.g., 1067 K for the $J = 4$ line.)

HCN is a well-known indicator of high gas density. Gao & Solomon (2004) demonstrated that a very strong linear correlation exists between the luminosities L_{IR} and L_{HCN} for mm-wave transitions of HCN, extending over a wide range of L_{IR} from normal galaxies to ULIRGs. They found the similar L_{IR}–L_{CO} correlation to have a less linear form, marking out L_{HCN} as the best tracer of dense molecular gas mass in galaxies, and hence of active star formation. However, Graciá-Carpio et al. (2008) present evidence that L_{IR}/L_{HCN} is systematically higher in (U)LIRGs than in normal star-forming galaxies. The relative line integrals from the $J = 4$ and 6 lines suggest an approximate excitation temperature of ∼150 K. These transitions represent high excitation, and given the complicated scenarios now emerging for the central region of Arp 220, it would be of great interest to ascertain the precise circumstances under which these absorptions arise.

Unlike the relatively "smooth" line profiles seen for the excited-OH lines (e.g. Figure 5), the HCN lines each show evidence for the presence of a number of discrete components. In fact, the central, strongest HCN component becomes increasingly dominant from $J = 4$ to 6. The absence of the $J = 2$ line requires explanation, as the predicted absorption line is expected to be an order of magnitude stronger than the 3σ limit we place above. It is highly improbable that the fraction of the continuum emission "covered" by the clouds producing the HCN absorption could have decreased by such a large amount between 4488 and 1347 MHz that the $J = 2$ line is rendered unobservable. Much more likely is that free–free absorption in the foreground ionized screen of this starburst galaxy greatly attenuates the $J = 2$ line. For this to be the case, an opacity of $\gtrsim$2.25 at 1347 MHz (in the rest frame of Arp 220) would be required. This would imply an optical depth of $\gtrsim$1.5 at 1630 MHz in the galaxy, as found for the spectra of a number of supernova remnants (SNRs) near the twin nuclei of Arp 220 by Parra et al. (2007). These authors attributed this high opacity to the combined presence of "a patchy FFA (free–free absorption) ISM with a median opacity of less than 1," plus absorption in the regions of ionized circumstellar mass-loss envelopes surrounding the SN progenitors. The HCN lines we see are expected to arise from star-forming regions of high gas density, and a detailed study of all possible lines in the $v_2 = 1$ direct l-type transitions of the HCN ladder would provide useful evidence concerning the properties of the foreground gas screen to these regions. Clearly, the spectrum of the HCN $J = 3$ line (with a rest frequency of 2693.3 MHz) will be crucial to such a study, and we will be observing this line during our 2008 campaign to complete the present observations. It should be noted that for the implied optical depths at 1347 MHz, even the $J = 4$ line will be reduced through FFA by $\gtrsim$20%, which would reduce the above-derived excitation temperature to ∼120 K.

4.3. Excited Hydroxyl (OH)

The energy levels for the various OH transitions are shown in Figure 4. In Figures 5–8, we present the λ6, 5, and 4 cm Λ-doublet transitions of the OH radical seen in absorption against the continuum emission of Arp 220. The relevant quantum numbers, rest frequencies, and other measured line parameters are presented in Table 2. The λ6 and 5 cm lines

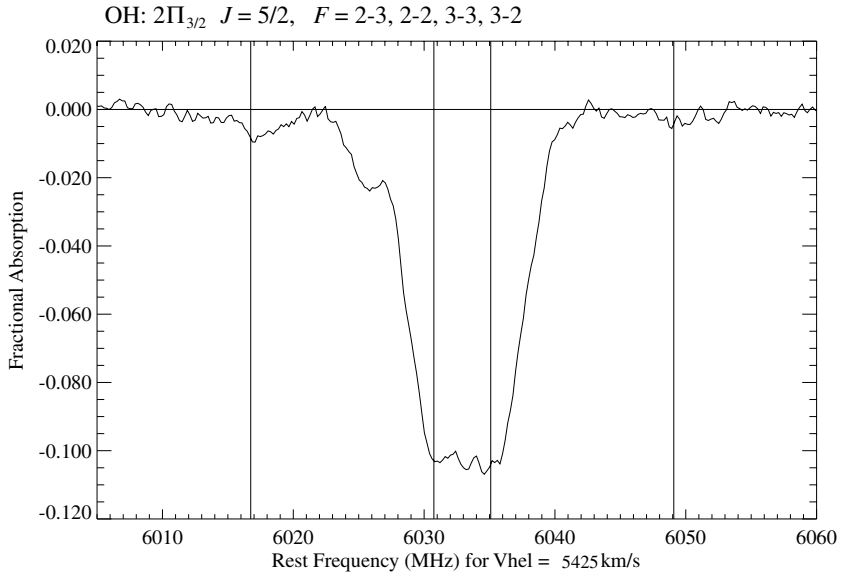

Figure 6. The four λ5 cm excited OH transitions as a function of rest frequency for an assumed heliocentric velocity of 5425 km s^{-1} (as appropriate for the λ6 cm OH lines). The frequencies of the four transitions $2\Pi_{3/2}$, $J = 5/2$, $F = 2$–3, 2–2, 3–3, and 3–2 are indicated by vertical lines. The two main lines form a blended absorption line profile. The velocity resolution is ∼30 km s^{-1}.

have been previously detected by Henkel et al. (1987, 1986) respectively.

Contrary to the findings of Henkel et al. (1987), we find that the 4660, 4751, and 4766 MHz lines have intensity ratios closely in agreement with their expected local thermodynamic equilibrium (LTE) values of 1:2:1.

The λ5 cm main lines presented here have a considerably higher S/N than the measurements of Henkel et al. (1986), but show a similar form. The expected LTE intensity ratios for the 6017, 6031, 6035, and 6049 MHz lines are 1:14:20:1, respectively. However, we measure ratios of 1:13:13:<0.4. The two main lines of the λ5 cm transition (6031 and 6035 MHz) are blended due to their large velocity widths and give the appearance of being "saturated," as suggested by their similar optical depths. This may be due to their having high optical depths, resulting in saturation of the lines against a continuum component containing of order 10% of the total flux density of Arp 220. However, we note that there is a low-velocity component to (presumably) the 6031 MHz absorption line, seen in Figure 6 at 6026 MHz, which if also present for the 6035 MHz line would contribute significantly to the frequency of the 6031 MHz line. The satellite lines are seen at a much lower S/N level. However, the greater strength of the 6017 MHz line relative to that at 6049 MHz is interesting. A similar effect was also found by Gardner & Martín-Pintado (1983) for four compact HII regions in our own Galaxy. While they saw the 6017 MHz lines enhanced above the LTE ratio to the main lines, the 6049 MHz line was weaker than predicted, and may even sometimes have appeared in weak emission.

The two λ4 cm OH lines at 7761 and 7820 MHz (Figure 7) are detected for the first time in Arp 220, and show velocity widths similar to most other molecular species in the galaxy. The expected ratio for these $2\Pi_{1/2}$, $J = 3/2$ main lines (7761:7820 MHz) is 1:1.8 in thermal equilibrium, very close to the derived ratio of the peak and integrated brightnesses for the lines of 1:1.89 (see Table 2). The satellite lines in this multiplet are expected to be present only at the 1σ level, and indeed are not detected. Considering the absorption lines in the $2\Pi_{1/2}$ ladder of Figure 4 at 4750 and 7820 MHz, in thermal equilibrium the ratio of their integrated optical depths would imply an excitation temperature of about 88 K. In a detailed Large Velocity Gradient (LVG) study of their CO observations, Greve et al. (2006) find that in Arp 220, the spectra of low-density tracers such as CO (and OH) can only be fitted with a two-phase molecular ISM with the kinetic temperature of one being >30 K, while their mm-wave spectra for the high-density tracer molecules, HCN and CS, indicate kinetic temperatures of ∼50–70 K.

A very tentative detection of the $2\Pi_{1/2}$, $J = 5/2$, $F = 2$–2 line of OH at 8135 MHz is shown in Figure 8. If confirmed by the addition of the remaining data to be acquired in this project, this would be at least twice as strong as expected for an excitation temperature of 88 K. Further, this line is expected to be only 0.7 times as strong as for the other $2\Pi_{1/2}$, $J = 5/2$ main line at 8189 MHz. While the 8189 MHz line is also possibly detected, contrary to expectations this would be at an even lower S/N level than for the 8135 MHz transition.

4.4. Formic Acid (HCOOH) or "Heavy" Hydroxyl (^{18}OH)

In Figure 9, we present a high S/N detection of an absorption line from our L-band spectrum. Despite the presence of nearby RFI caused by Glonass emissions (at ∼1605 MHz), the reality of this absorption line has been verified by its presence with similar optical depth in each of 13 individual spectra of Arp 220, but in none of the spectra of the bandpass calibrator. As demonstrated by the horizontal lines in Figure 9, there is an ambiguity as to the species responsible for this absorption, which could be either the 1639.5 MHz main line of ^{18}OH or the 1638.8 MHz line of formic acid (HCOOH). Given the prevalence of OH in Arp 220, it would perhaps not be unreasonable to detect the presence of ^{18}OH as well. However, since formic acid is relevant to the chemical origin of life, it would be most interesting to resolve this ambiguity.

As is seen in Figure 9, as well as the strong absorption line detected near 1611 MHz, an apparently weaker absorption

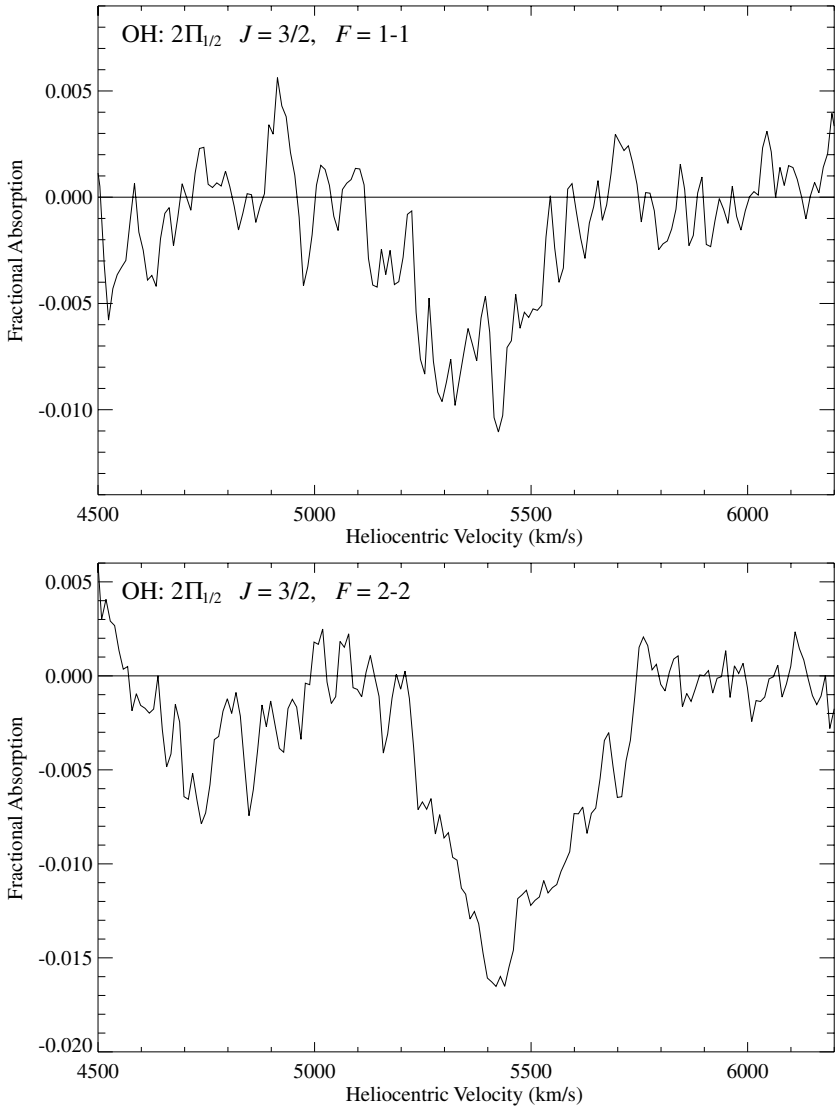

Figure 7. First detections of the two λ4 cm excited OH main-line transitions, $2\Pi_{1/2}$, $J = 3/2$, $F = 1$–1 and 2–2 (at 7761 and 7820 MHz respectively). The spectra are plotted with heliocentric velocity as abscissa. The velocity resolution is ∼30 km s^{-1}.

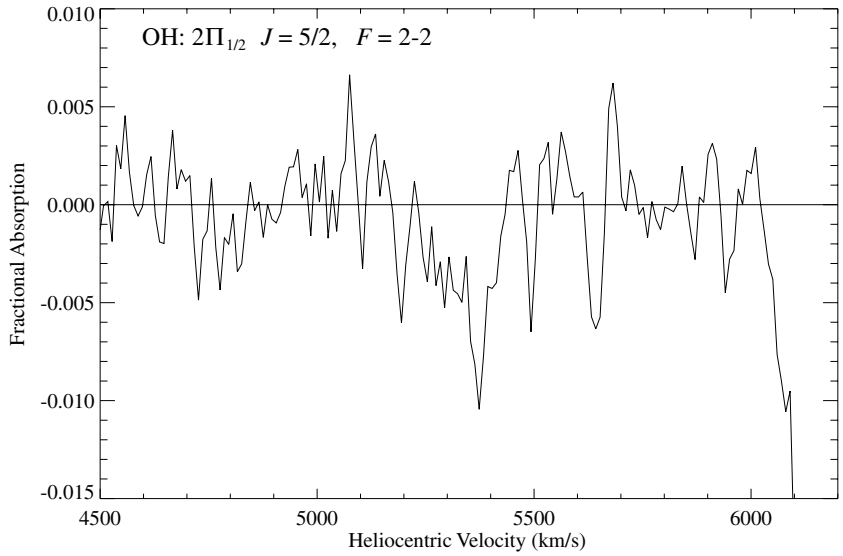

Figure 8. A possible detection of the λ4 cm excited OH transition $2\Pi_{1/2}$, $J = 5/2$, $F = 2$–2 (at 8135 MHz). The spectrum is plotted with heliocentric velocity as abscissa. The velocity resolution is ∼30 km s^{-1}.

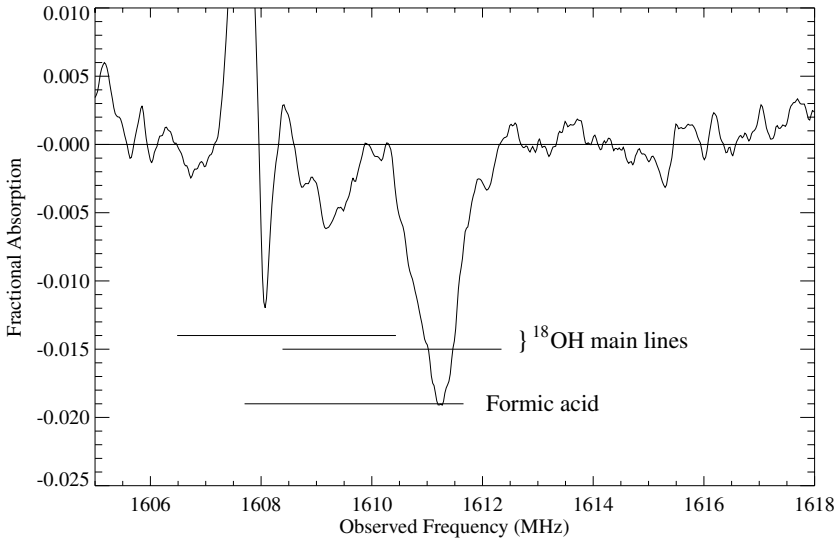

Figure 9. This plot shows one (or possibly two) absorption line(s) that could be either formic acid or ^{18}OH. The expected location of the formic acid line and of the two main ^{18}OH lines are indicated with horizontal bars. The band is affected by interference from the Glonass system at about 1605 MHz, but the authenticity of the deep absorption feature has been verified by its non-appearance in the spectra of the bandpass calibrator. The velocity resolution is ∼30 km s^{-1}.

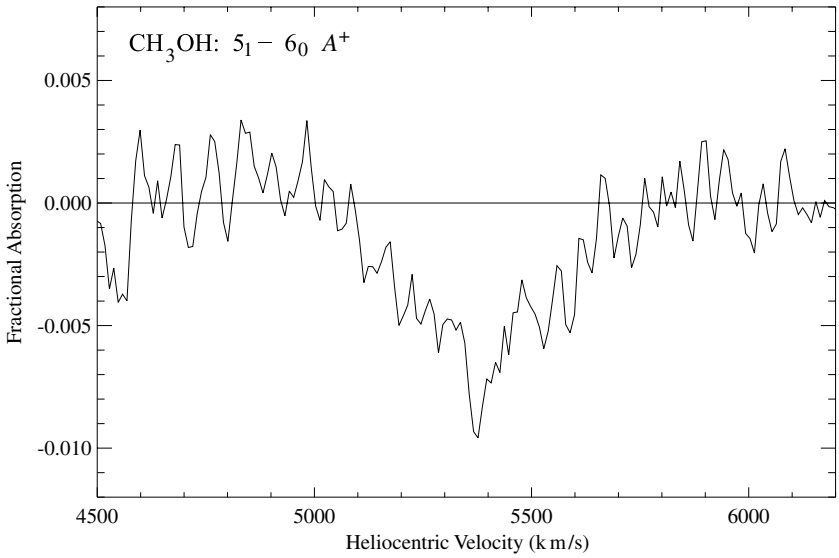

Figure 10. A possible detection of the 5_1–6_0 A^+ methanol line (at 6668 MHz) in absorption. However, more data are needed to confirm the detection. The spectrum is plotted with heliocentric velocity as abscissa. The velocity resolution is ∼30 km s^{-1}.

is also seen near 1609 MHz, close to where the second, 1637.6 MHz, main line of ^{18}OH should be found. If this feature were indeed to be real, the ratio of the peak intensity of the higher-frequency absorption to this would be 3.1:1. This is higher than the expected ratio of 1.8:1 were the pair to be the main lines of ^{18}OH (Barrett & Rogers 1964) and in local thermal equilibrium. The frequencies of the peak depths of the two features are separated by an amount that would correspond to a rest frequency separation of about 2.05 MHz were they both to be due to absorption in Arp 220. The laboratory separation of the ^{18}OH main lines is 1.939 ± 0.003 MHz (Lovas 1986), and hence given the weakness of the feature near 1609 MHz, the agreement is considered to be satisfactory.

If the absorption near 1611 MHz is indeed the higher-frequency component of the ^{18}OH main lines, then its radial velocity is closer to that of the peak velocity found for other molecules in Arp 220 than would be the case were the detection to be of formic acid (see Table 2 and the horizontal bars displayed in Figure 9.) However, even for ^{18}OH, this velocity of ∼5265 km s^{-1} is significantly lower than that of the normal molecular peak velocity in Arp 220. In addition, its width of about 190 km s^{-1} is narrower than for any other species that we detect. Were this absorbing gas to represent ^{18}OH, we note that a velocity of 5265 km s^{-1} is "allowed" in Arp 220 from the HI absorption study of Mundell et al. (2001). However, a peak velocity of 5135 km s^{-1}, appropriate for the formic acid transition, has little associated HI absorption. Nevertheless, if the absorption were to be due to ^{18}OH at 5265 km s^{-1} this would imply a remarkably high isotopic ratio of ^{18}OH:^{16}OH for a cloud at this velocity, especially so as this is well away from the peak velocity range of the OH megamaser line as seen at low angular resolution (Baan et al. 1982).

Given the proximity of the Glonass RFI, it is difficult to establish the origins of this absorption feature. However, ^{18}OH would seem a more likely identification than formic acid. Confirmation of the reality of the second, weaker, absorption component near

1609 MHz would effectively establish this identification. The possibility that the feature represents absorption in our Galaxy from the 1612.231 MHz satellite OH line has to be very small given the high Galactic latitude of the line of sight ($b = 53^\circ.0$), the implied large radial velocity ($\sim$+185 km s^{-1}), and large line width ($\sim$190 km s^{-1}).

4.5. Methanol (CH_3OH)

In Figure 10, we present a possible detection of the 5_1–6_0 A^+ methanol line in absorption. Although this line is apparently detected with an S/N of almost 6:1, and the entire 100 MHz band in which it is observed is basically RFI-free, the quality of the baseline in this case is rather poor. We await our remaining observations for confirming the reality of this line. We note that while the excited-OH absorption line at 7761.7 MHz (Figure 7: upper) has a somewhat lower S/N than this possible methanol detection, the combination of a better overall baseline, and the 10.5σ level detection of the associated line at 7820.1 MHz (Figure 7: lower) yielding the expected LTE intensity ratio (see Section 4.3), makes for a more solid detection in that case. We can certainly conclude that at the 1 mJy level (5σ) no methanol maser emission, such as is commonly detected for this transition from regions of massive-star formation in our own Galaxy, is seen in Arp 220.

Assuming the reality of the methanol absorption line, an excitation temperature for the transition of $T_{\rm ex} = 20$ K, and an Einstein coefficient of $A = 0.1532 \times 10^{-8}$ s^{-1} (Cragg et al. 1993), and a covering factor of unity, in LTE the column density of the lower energy level, $N_{6,0}$, is

$$N_{6,0} = 1.34 \times 10^{15} \int \tau \delta v \ {\rm cm}^{-2}, \quad (1)$$

where the integral $\int \tau \delta v$ is expressed in units of km s^{-1}.

An approximation for the total column density of methanol can be obtained assuming a Boltzmann distribution for the methanol energy-level population. If the relative abundances of the A and E species of this molecule are taken to be 1:1 based on their having a relatively small ground-state energy difference, then the total column density of methanol molecules is

$$N = N_{6,0} 2/13 Q(T_{\rm ex}) e^{\frac{E_{6,0}}{kT_{\rm ex}}}, \quad (2)$$

where $Q(T_{\rm ex})$ is the partition function, taken to be 39.8 (D. Cragg, quoted in Houghton & Whiteoak 1995), and $E_{6,0}$ is the energy above the ground state of the 6_0A^+ level. Thus, the presence of a 6668 MHz methanol absorption line in Arp 220 would imply a total column density for this molecule of $N_{\rm CH_3OH} \sim 2.5 \times 10^{17}$ cm^{-2}.

5. CONCLUDING REMARKS

The Arecibo Arp 220 Spectral Census is an on-going project and a detailed analysis will be presented in a separate paper, as will the final spectra from the completed project. We have presented here the discovery of methanimine in this galaxy and the detection of three previously unseen cm-wavelength transitions of HCN. We have also observed, for the first time in Arp 220, an absorption line that may be either formic acid or ^{18}OH, two (possibly three) λ4 cm transitions of excited OH, and what may be the first extragalactic detection of methanol.

The discovery of high abundances of "pre-biotic" molecules, such as methanimine, HCN, and possibly formic acid in Arp 220 raises the possibility that other ULIRGs might similarly contain high abundances of such molecules, which could be detectable with the Arecibo 305 m telescope.

We thank Paul Goldsmith (JPL), Sven Thorwirth, and Karl Menten (MPIfR) for fruitful discussions, and an anonymous referee for a number of useful suggestions which considerably improved the paper. The Arecibo Observatory is a part of the National Astronomy and Ionosphere Center (NAIC) operated by Cornell University under a cooperative agreement with the National Science Foundation (NSF).

Facilities: Arecibo (L-wide, S-high, C, C-high, X)

REFERENCES

Araya, E., Baan, W. A., & Hofner, P. 2004, ApJS, 154, 541
Armus, L., et al. 2007, ApJ, 656, 148
Baan, W. A. 1989, ApJ, 338, 804
Baan, W. A., & Haschick, A. D. 1995, ApJ, 454, 745
Baan, W. A., Wood, P. A. D., & Haschick, A. D. 1982, ApJ, 260, L49
Barrett, A. H., & Rogers, A. E. E. 1964, Nature, 204, 62
Blagojevic, V., Petrie, S., & Bohme, D. K. 2003, MNRAS, 339, L7
Caselli, P., Hasegawa, T. I., & Herbst, E. 1993, ApJ, 408, 548
Cragg, D. M., Mikhtiev, M. A., Bettens, R. P. A., Godfrey, P. D., & Brown, R. D. 1993, MNRAS, 264, 769
Darling, J., & Giovanelli, R. 2002, AJ, 124, 100
Diamond, P. J., Norris, R. P., Baan, W. A., & Booth, R. S. 1989, ApJ, 340, L49
Dickens, J. E., Irvine, W. M., DeVries, C. H., & Ohishi, M. 1997, ApJ, 479, 307
Dickerson, R. E. 1978, Sci. Am., 239, 70
Downes, D., & Eckart, A. 2007, A&A, 468, L57
Elsila, J. E., Dworkin, J. P., Berstein, M. P., Martin, M. P., & Sanford, S. A. 2007, ApJ, 660, 911
Elston, R., Cornell, M. E., & Lebofsky, M. J. 1985, ApJ, 296, 106
Evans, A. S., Solomon, P. M., Tacconi, L. J., Vavilkin, T., & Downes, D. 2006, AJ, 132, 2398
Gao, Yu., & Solomon, P. M. 2004, ApJS, 152, 63
Gardner, F. F., & Martín-Pintado, J. 1983, MNRAS, 204, 709
Genzel, R., et al. 1998, ApJ, 498, 579
Ghosh, T., & Salter, C. J. 2002, in ASP Conf. Ser. 278, Single-Dish Radio Astronomy: Techniques and Applications, ed. S. Stanimirovic, D. Altschuler, P. Goldsmith, & C. Salter (San Francisco, CA: ASP), 521
Ghosh, T., Kavars, D. W., Robinson, P. E., Saintonge, A., Strasser, S. T., & Salter, C. J. 2003, BAAS, 35, 1393
Godfrey, P. D., Brown, R. D., Robinson, B. J., & Sinclair, M. W. 1973, Astrophys. Lett., 13, 119
Graciá-Carpio, J., García-Burillo, S., Planesas, P., Fuente, A., & Usero, A. 2008, A&A, 479, 703
Greve, T. R., Papadopoulos, P. P., Gao, Y., & Radford, S. J. E. 2006, arXiv astro-ph/0610378
Henkel, C., Güsten, R., & Baan, W. A. 1987, A&A, 185, 14
Henkel, C., Güsten, R., & Batrla, W. 1986, A&A, 168, L13
Houghton, S., & Whiteoak, J. B. 1995, MNRAS, 273, 1033
Imanishi, M., Dudley, C. C., Maiolino, R., Maloney, P. R., Nakagawa, T., & Risaliti, G. 2007a, ApJS, 171, 72
Imanishi, M., Nakanishi, K., Tamura, Y., Oi, N., & Kohno, K. 2007b, AJ, 134, 2366
Kennicutt, R. C. 1998, ARAA, 36, 189
Kirchoff, W. H., Johnson, D. R., & Lovas, F. J. 1973, J. Phys. Chem. Ref. Data, 2, 1
Lawrence, A., Walker, D., Rowan-Robinson, M., Leech, K. J., & Penston, M. V. 1986, MNRAS, 219, 687
Lonsdale, C. J., Diamond, P. J., Smith, H. E., & Lonsdale, C. J. 1998, ApJ, 493, L13
Lonsdale, C. J., Diamond, P. J., Thrall, H., Smith, H. E., & Lonsdale, C. J. 2006, ApJ, 647, 185
Lovas, F. J. 1986, J. Phys. Chem. Ref. Data, 15, 251
Lutz, D., Veilleux, S., & Genzel, R. 1999, ApJ, 517, L13
Martin, J. M., Le Squeren, A. M., Bottinelli, L., Gouguenheim, L., & Dennefeld, M. 1989, A&A, 208, 39
Martín, S., Mauersberger, R., Martín-Pintado, J., Henkel, C., & García-Burillo, S. 2006, ApJS, 164, 450
Momjian, E., Romney, J. D., Carilli, C. L., & Troland, T. H. 2006, ApJ, 653, 1172

Müller, H. S. P., Schlöder, F., Stutzki, J., & Winnewisser, G. 2005, J. Mol. Struct., 742, 215
Müller, H. S. P., Thorwirth, S., Roth, D. A., & Winnewisser, G. 2001, A&A, 370, L49
Mundell, C. G., Ferruit, P., & Pedlar, A. 2001, ApJ, 560, 168
Nguyen, M. T., Sengupta, D., & Ha, T.-K. 1996, J. Phys. Chem., 100, 6499
Nomura, H., & Millar, T. J. 2004, A&A, 414, 409
Parra, R., Conway, J. E., Diamond, P. J., Thrall, H., Lonsdale, C. J., Lonsdale, C. J., & Smith, H. E. 2007, ApJ, 659, 314
Parra, R., Conway, J. E., Elitzur, E., & Pihlström, Y. M. 2005, A&A, 443, 383
Rovilos, E., Diamond, P. J., Lonsdale, C. J., Lonsdale, C. J., & Smith, H. E. 2003, MNRAS, 342, 373
Sakamoto, K., Scoville, N. Z., Yun, M. S., Crosas, M., Genzel, R., & Tacconi, L. J. 1999, ApJ, 514, 68
Sanders, D. B., & Mirabel, I. F. 1996, ARA&A, 34, 749
Scoville, N. Z., Sanders, D. B., Sargent, A. I., Soifer, B. T., Scott, S. L., & Lo, K. Y. 1986, ApJ, 311, L47
Scoville, N. Z., et al. 2000, AJ, 119, 991
Solomon, P. M., Downes, D., & Radford, S. J. E. 1992, ApJ, 387, L55
Surace, J. A., & Sanders, D. B. 1999, ApJ, 512, 162
Takano, S., Nakanishi, K., Nakai, N., & Takano, T. 2005, PASJ, 57, L29
Thorwirth, S., Wyrowski, F., Schilke, P., Menten, K. M., Brünken, S., Müller, H. S. P., & Winnewisser, G. 2003, ApJ, 586, 338
Veilleux, S., Kim, D.-C., & Sanders, D. B. 2002, ApJS, 143, 315
Veilleux, S., et al. 2006, ApJ, 643, 707